Eur. Phys. J. E (2016) **39**: 116
DOI 10.1140/epje/i2016-16116-4

THE EUROPEAN PHYSICAL JOURNAL E

Regular Article

Ratchet effect for two-dimensional nanoparticle motion in a corrugated oscillating channel

Matthias Radtke and Roland R. Netz[a]

Department of Physics, Freie Universität Berlin, Arnimallee 14, 14195 Berlin, Germany

Received 22 September 2016 and Received in final form 28 October 2016
Published online: 30 November 2016 – © EDP Sciences / Società Italiana di Fisica / Springer-Verlag 2016

Abstract. The motion of a single rigid or elastic particle inside a corrugated narrow channel is investigated by means of Brownian dynamics simulations. Periodic oscillations of one of the asymmetric channel surfaces induce directed particle transport. For different surface structures of the resting channel surface, we determine optimal transport properties in terms of the driving frequency, particle size, and corrugation amplitude. The transport direction is changed when switching from perpendicular motion of the oscillating surface to parallel motion with respect to the resting surface, which can be rationalized by a transition from a flashing to a pushing ratchet effect. We also study the diffusion behavior and find strongly enhanced diffusion for parallel oscillatory motion with a diffusivity significantly larger than for free diffusion. Elastic large particles exhibit suppressed transport with increasing rigidity. In contrast, for small particles, increasing rigidity enhances the particle transport both in terms of particle velocity and diffusivity.

1 Introduction

The so-called ratchet effect describes the directed Brownian motion of particles generated by a non-equilibrium perturbation of a periodic system. One necessary ingredient is that the spatial symmetry is broken in order to single out one direction over the other [1–8]. Ratchet-shaped surfaces are observed in a number of different biological systems ranging from biopolymers [9,10] such as actin [11], the cuticular structure of hair [12], to macroscopic systems [13,14] like plants [15]. A different class of ratchet systems is constituted by self-propelled swimmers on asymmetric substrates, where motion is rectified by active particles instead of external driving [16]. Yet another example of rectified transport is the Tesla valve, already patented in 1916, where an asymmetrically shaped pipe allows for a fluid to flow preferentially in one direction, an effect that is due to the onset of turbulent flow [17]. This whole field presents an area of active research, as ratchet effects and the resulting net current can be utilized for applications like cargo transport, *e.g.* in drug delivery systems [18], or for separation and sorting of nanoparticles [19].

In this study, we introduce a geometric two-dimensional ratchet model and investigate the transport properties of a single diffusing nanoparticle inside a narrow corrugated channel. One of the channel surfaces is modeled as an asymmetric surface and subject to oscillatory motion. The other channel surface is resting and has varying surface structures. This model is inspired by nanoparticle transport into hair follicles [12,20], where it has been hypothesized that the cuticular hair surface structure causes a ratchet effect and rectifies nanoparticle motion toward the hair root induced by motion of the hair [21,22]. We study transport properties of the nanoparticle under periodic motion of the oscillating surface in perpendicular and parallel direction with respect to the resting surface. For varying frequencies of perpendicular motion, we find directed particle motion with an optimal driving frequency. We also find a slight enhancement of the particle diffusivity. We observe reversal of the transport direction when changing the surface oscillation mode from perpendicular to parallel. For parallel motion, a significant enhancement of the diffusion is observed with diffusivities larger than for free diffusion. Studying the influence of the particle size and corrugation amplitude of the oscillating surface on the transport efficiency, we determine an optimal particle size and an optimal corrugation amplitude. We also study elastic nanoparticles and find that for large particle sizes, comparable to the surface separation, elasticity leads to more efficient particle transport. In contrast, for small particles efficient transport is observed when the rigidity is large. The first section introduces the model and details the Brownian dynamics simulations. In the last section we conclude with a short summary.

[a] e-mail: rnetz@physik.fu-berlin.de

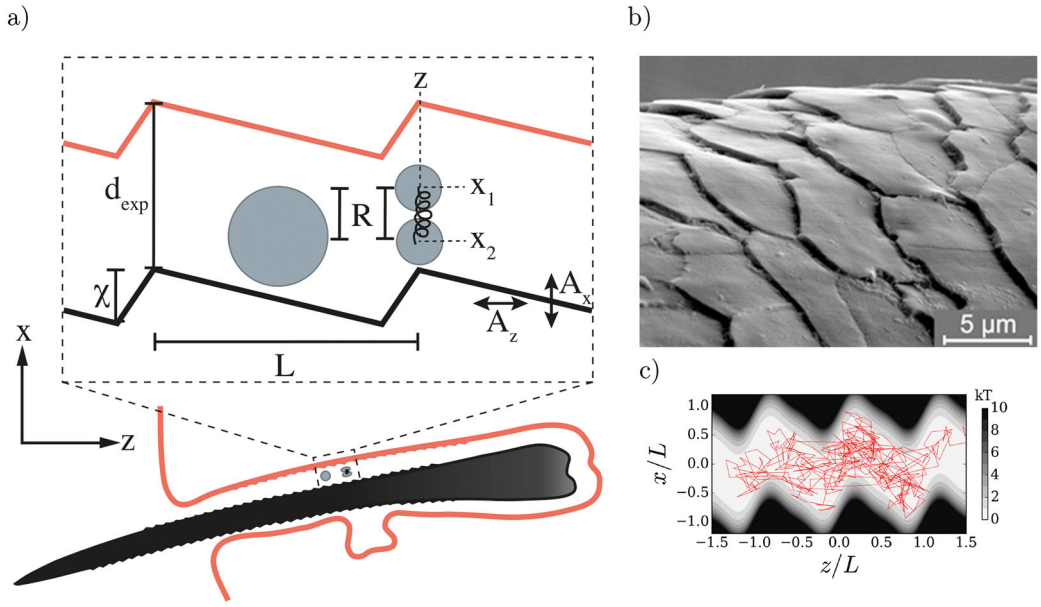

Fig. 1. (a) Schematic illustration of a nanoparticle inside a narrow corrugated channel. The particle (grey) of radius R is either rigid (left) or elastic (right) consisting of two subunits that are vertically connected by a spring. The lower oscillating surface (black) and the upper resting surface (red) are separated by a distance $d_{\rm exp}$ and exhibit the same corrugation amplitude χ and the same periodicity L. Surface oscillations are either perpendicular with amplitude A_x or parallel with amplitude A_z. A biological example for such a narrow channel is the space between a hair and the follicle. (b) Electron microscopic image of the cuticular structure of the human terminal hair [24]. (c) Contour plot of the potential energy equation (4) in units of kT for the rescaled model parameters $d/L = 1.0$, $\chi/L = 0.3$, $m = 1$. The red trajectory illustrates the Brownian motion of a nanoparticle in the absence of external driving.

2 Model and simulation details

The motion of a single nanoparticle inside a narrow channel is modeled in two dimensions interacting with an externally driven corrugated oscillating surface and an opposing resting surface with different surface structures. As schematically depicted in fig. 1(a), we use an asymmetric sawtooth structure to represent the lower oscillating surface. A biological example is the cuticular hair surface, shown in fig. 1(b), for which the resting surface (shown in red) in fig. 1(a) corresponds to the inner root sheath, *i.e.* the innermost layer of the hair follicle. By interlocking of the cuticular hair surface with the oppositely oriented cuticle cells of the inner root sheath, the hair is anchored in the follicle [23].

For a general model, the sawtooth structure of the oscillating and the resting surface, shown in fig. 1(a) in black and red, respectively, are characterized by the corrugation amplitude χ and the periodicity L. Note that in the first part the rigid nanoparticle is modeled as point-like and we neglect deformational and rotational degrees of freedom. The effect of different particle sizes is taken into account in our simulations via the surface separation d. In order to connect to the experimental situation, the experimental distance between the hair and the follicle surfaces is defined as $d_{\rm exp} = d + 2R$ and thus effectively incorporates the effect of changing particle radius R.

We model the repulsion of the nanoparticle from the two surfaces, separated by the distance d, employing exponentially decaying potentials located on the oscillating surface and the resting surface

$$U_{\rm osc}(x) = e^{-\frac{x+d/2-A_x \sin \omega t}{\kappa}}, \tag{1}$$

$$U_{\rm res}(x) = e^{\frac{x-d/2}{\kappa}}, \tag{2}$$

with a short rescaled surface interaction range $\kappa/L = 0.2$. The oscillating surface is externally driven either into perpendicular motion with respect to the channel axis, or into parallel motion. Perpendicular ratchet motion, illustrated in fig. 2(b), is included in our model via the time-dependent periodic term in the potential equation (1) with frequency ω and amplitude A_x. The sawtooth shape of the potential energy landscape is achieved with a ratchet shape function [25] given by

$$F(z) = -\chi \left[\sin(2\pi z/L) + \frac{1}{4}\sin(4\pi z/L)\right]. \tag{3}$$

The total potential energy reads

$$U(x,z) = U_{\rm osc}\left(x + F\left(z + A_z \sin \omega t\right)\right) + U_{\rm res}\left(x + F(m \cdot z)\right), \tag{4}$$

where we introduce a structure parameter $m = -1, 0, 1$ as well as the periodic parallel motion of the oscillating surface with amplitude A_z, which is illustrated in fig. 4(b). We introduce the parameter m in order to study the effect of different structures of the resting surface. For the example of hair, this can represent the different follicle surface

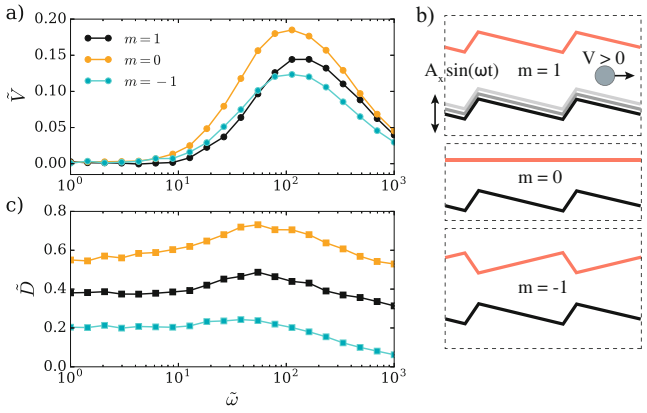

Fig. 2. Results for a rigid particle subject to perpendicular motion of the oscillating surface with amplitude $\tilde{A}_x = 0.5$ (while $\tilde{A}_z = 0$) shown for the three different resting surface structures illustrated in (b) from top to bottom: interlocked case $m = 1$ (black symbols), flat case $m = 0$ (orange symbols), and symmetric case $m = -1$ (cyan symbols). The corrugation amplitude is fixed to $\tilde{\chi} = 0.5$ and the surface separation is $\tilde{d} = 1$. (a) The average rescaled velocity $\tilde{V}$ exhibits a maximum at a rescaled frequency $\tilde{\omega} \approx 100$. The position of the maximum slightly depends on the structure parameter m. The largest velocity is achieved for the flat case, $m = 0$, for which also the rescaled diffusivity $\tilde{D}$ in (c) is the largest. The diffusivity only weakly depends on $\tilde{\omega}$ for $m = -1$ and slightly decreases for large frequencies. A more pronounced maximum in the diffusivity is observed for $m = 0$ and $m = 1$ at a frequency $\tilde{\omega} \approx 50$ which is slightly smaller than the frequency corresponding to the maximum in the average velocity $\tilde{V}$ seen in (a).

structures, as the cuticle structure of the follicle presumably changes towards the root from a sawtooth shape to a relatively smooth surface [26]. We investigate three different resting surface structures as illustrated in fig. 2(b) from top to bottom: the interlocked case, $m = 1$, the flat case, $m = 0$, and the symmetric case with respect to the channel axis, $m = -1$. A contour plot of the potential energy, eq. (4), is shown in fig. 1(c) for the interlocked case, $m = 1$, with rescaled parameters $d/L = 1.0$ and $\chi/L = 0.3$, where a red trajectory illustrates the Brownian motion of a nanoparticle.

We perform Brownian dynamics simulations based on the overdamped Langevin equation,

$$\dot{x} = -\mu_0\, \partial_x U(x,z) + \xi_x(t)$$

$$\dot{z} = -\mu_0\, \partial_z U(x,z) + \xi_z(t), \tag{5}$$

which describes the diffusion of the particle in the perpendicular x-direction as well as in the parallel z-direction. The first term in eq. (5) accounts for the direct force acting on the particle with mobility μ_0 and the second term represents the stochastic contribution ξ_α given by Gaussian random components with correlations according to the fluctuation-dissipation theorem, $\langle \xi_\alpha(t)\xi_\beta(t')\rangle = 2\mathrm{kT}\,\mu_0\,\delta_{\alpha\beta}\delta(t-t')$, with $\alpha, \beta = x, z$, and vanishing mean. Note that in our model we assume the fluid background to be at rest, so we neglect any back-flow effects that might be caused by the oscillatory motion of the surface and which could influence the particle motion. We also neglect the possible adhesion of the particle on the surfaces, which in the case of cargo transport by microtubuli has been found to give rise to interesting transport properties [10].

In the following all quantities used are made dimensionless by rescaling lengths according to $\tilde{x} = x/L$ by the periodic length scale of the sawtooth structure L, energies $\tilde{U} = U/\mathrm{kT}$ by thermal energy and times $\tilde{t} = t/\tau$ by the characteristic particle diffusion time $\tau = L^2/\mu_0\mathrm{kT} = 6\pi\eta R\, L^2/\mathrm{kT}$ with viscosity η. For one set of parameters the simulation typically runs for 10^9 time steps with a rescaled time step $\Delta t/\tau = 10^{-4}$. From the simulations we obtain the average parallel velocity $V = \langle (x(t + 10^3\Delta t) - x(t))/(10^3\Delta t)\rangle$ by sampling the particle position every 10^3 steps as well as the diffusivity D by calculation of the mean square displacement

$$\left\langle (x(t) - x(0))^2 \right\rangle = 2Dt + V^2t^2. \tag{6}$$

In this study we also consider elastic nanoparticles and the effect of rigidity ζ on the transport properties. As schematically illustrated in fig. 1(a) (right), we model elastic nanoparticles as a dumbbell consisting of two nanoparticle subunits that are vertically connected by a harmonic spring of length R and spring constant ζ. Note that the dumbbell cannot rotate and thus only represents the vertical nanoparticle elasticity. The nanoparticle is now described by two vertical positions x_1 and x_2, while the position z along the parallel direction is the same for both subunits. The corresponding Langevin equation is given by

$$\dot{x} = -\mu_0\, \partial_x U_{\mathrm{el}} + \xi_x(t), \tag{7}$$

$$\dot{z}_1 = -\mu_0\, \partial_{z_1} U_{\mathrm{el}} + \xi_{z_1}(t), \tag{8}$$

$$\dot{z}_2 = -\mu_0\, \partial_{z_2} U_{\mathrm{el}} + \xi_{z_2}(t), \tag{9}$$

where the potential energy for the elastic nanoparticle is defined by

$$U_{\mathrm{el}} = U(x,z_1) + U(x,z_2) - \frac{\zeta}{2}\left(|z_1 - z_2| - R\right)^2. \tag{10}$$

3 Results

3.1 Transport properties of a rigid particle

First we study the particle transport for perpendicular motion of the oscillating surface as a function of the rescaled driving frequency $\tilde{\omega} = \omega\tau$ with fixed amplitude $\tilde{A}_x = 0.5$ (while $\tilde{A}_z = 0$). This situation is schematically depicted in the top of fig. 2(b). The distance $\tilde{d} = 1$ between the oscillating and resting surface is fixed and the corrugation amplitude is set to $\tilde{\chi} = 0.5$. Results for the average velocity $\tilde{V}$ and diffusivity $\tilde{D}$ are shown in figs. 2(a), (c) for different values of the structure parameter $m = -1, 0, 1$ with the corresponding resting surface structures shown in

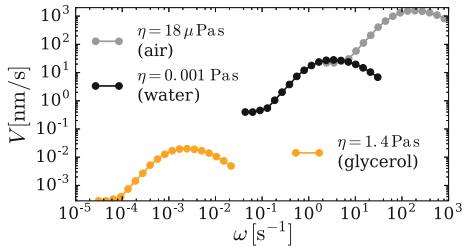

Fig. 3. Demonstration of how the rescaled simulation results in fig. 2a (for $m = 0$) of the average transport velocity V translate to physical units. The assumed physical parameters are corrugation length $L = 5\,\mu$m, corrugation amplitude $\chi = 2.5\,\mu$m, nanoparticle radius $R = 0.3\,\mu$m, surface separation $d = 5\,\mu$m, oscillation amplitude $A_x = 2.5\,\mu$m ($A_z = 0$), and temperature $T = 310$ K. When choosing different fluid viscosities corresponding to air (grey), water (black), and glycerol (orange symbols), both the optimal driving frequency ω of the perpendicularly oscillating surface as well as the resulting transport velocity vary by several orders of magnitude.

fig. 2(b). We find enhanced particle transport to the right induced by the perpendicular ratchet motion, as seen from the positive average velocity in fig. 2(a) as a function of frequency. There is an optimal frequency at which the average velocity exhibits a maximum, the position and magnitude of which depends on the resting surface structure. The largest velocity is achieved for the flat case, $m = 0$. The interlocked case, $m = 1$, leads to slightly larger velocities compared to the symmetric case, $m = -1$. As shown in fig. 2(c), the largest diffusivity $\tilde{D}$ is observed for $m = 0$, with a maximum at somewhat smaller values of $\tilde{\omega}$ compared to the optimal frequency of the average velocity shown in fig. 2(a). For $m = 0$, at intermediate frequency the diffusivity exceeds the equilibrium value $\tilde{D} = 0.6$ obtained in the absence of oscillation (limit $\tilde{\omega} \to 0$ or $\tilde{A}_x \to 0$). The smallest diffusivity is observed for $m = -1$ with a weak dependence on the frequency; for large $\tilde{\omega} > 100$ the diffusivity monotonically decreases for all values of m.

In order to be able to compare our simulations with experiments, we present in fig. 3 the average transport velocity in physical units as a function of the perpendicular driving frequency, which is the same data already shown in fig. 2(a) for $m = 0$. For this plot we assume a characteristic corrugation length scale $L = 5\,\mu$m, which corresponds to the length scale of the cuticular hair structure in fig. 1(a), a corrugation amplitude $\chi = 2.5\,\mu$m, and a particle radius $R = 0.3\,\mu$m. Simulation results in fig. 3 are shown for a temperature $T = 310$ K and three different viscosities: the viscosity of air, $\eta = 18\,\mu$Pa s, the viscosity of water, $\eta = 0.001$ Pa s, and the viscosity of glycerol, $\eta = 1.4$ Pa s. It can be seen that the optimal frequency and the resulting transport velocity strongly depend on the system viscosity. For the case of nanoparticle motion in the hair follicle, we conclude that the local fluid viscosity inside the hair follicle is a very important parameter that sensitively influences the directed particle transport properties. When we assume a local viscosity close to that

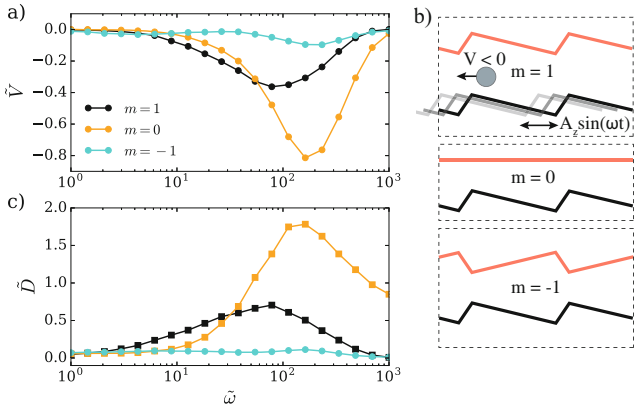

Fig. 4. Results for a rigid particle subject to parallel motion of the oscillating surface with amplitude $\tilde{A}_z = 0.5$ (while $\tilde{A}_x = 0$) for fixed $\tilde{\chi} = 0.5$ and $\tilde{d} = 0.2$. (a) For the interlocked case, $m = 1$, (black symbols) the average rescaled velocity $\tilde{V}$ is negative and decreases with increasing the frequency and exhibits a minimum at $\tilde{\omega} \approx 80$. A flat resting surface $m = 0$, (orange symbols) induces larger negative velocities with a minimum at $\tilde{\omega} \approx 160$. For $m = -1$ (cyan symbols) the particle transport is less pronounced. (b) Illustration of the different resting surface structures. (c) The diffusivity as a function of frequency exhibits for $m = 1$ and $m = 0$ a maximum at a frequency corresponding to the minimum in average velocity shown in (a). Diffusivities larger than for free diffusion $\tilde{D} > 1$ are observed for a flat resting surface, $m = 0$. For the case $m = -1$, the diffusivity only weakly depends on the frequency.

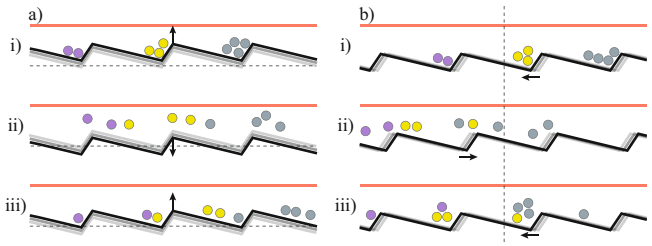

Fig. 5. (a) Illustration of perpendicular ratchet motion and the flashing ratchet effect that leads to transport of the nanoparticles to the right, *i.e.* down the shallow slopes. i) Upward motion leads to strong particle localization in the potential minima. Subsequent downward motion in ii) allows relaxation and particle diffusion from the minima over the barriers with the steep slope. Transport to the right results in iii) from upwardly moving the surface that pushes some particles down the shallow slopes. (b) Illustration of the parallel ratchet motion and the pushing ratchet effect that leads to transport of the nanoparticles to the left. i) The oscillating surface moves to the left and the steep slopes push particles to the left. ii) Ratchet motion to the right has a less pronounced effect on the particles, which can diffuse over the flanks with the shallow slope to the left. iii) Subsequent leftward ratchet motion again leads to localization and forced motion of the particles to the left.

of water, our simulation results suggest maximal transport velocities of about 30 nm/s at frequencies of a few Hertz.

Next we consider the parallel motion of the oscillating surface as schematically shown in fig. 4(b). The average velocity and the diffusivity of a rigid particle are presented in figs. 4(a), (c) as a function of frequency $\tilde{\omega}$ for

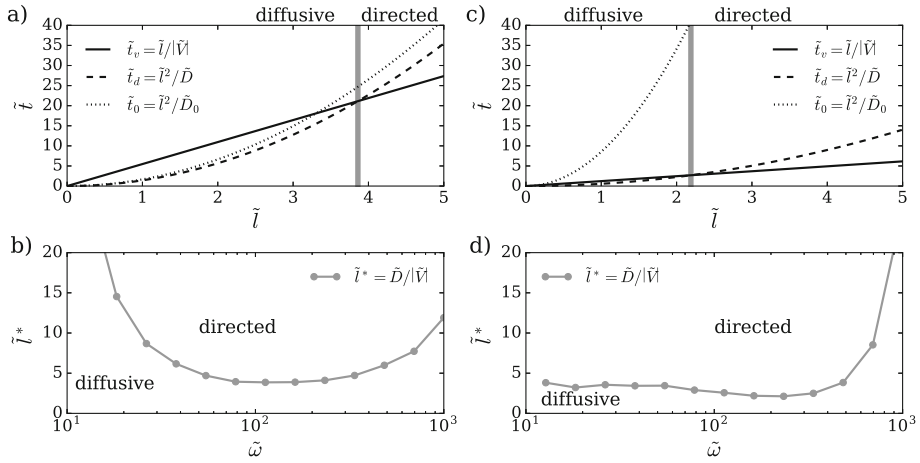

Fig. 6. Comparison of directed transport and diffusive transport of a rigid particle for fixed parameters $\tilde{\chi} = 0.5$ and $m = 0$. (a) The characteristic time scale for directed motion $\tilde{t}_v = \tilde{l}/|\tilde{V}|$ (solid line) and diffusive motion $\tilde{t}_d = \tilde{l}^2/\tilde{D}$ (dashed line) as a function of transport length $\tilde{l}$. For perpendicular ratchet motion with amplitude $\tilde{A}_x = 0.5$ and a surface separation of $\tilde{d} = 1$, as seen in fig. 2(a), we find the maximal particle velocity $\tilde{V} = 0.18$ at $\tilde{\omega} = 113$, where $\tilde{D} = 0.7$. The dotted line shows the time scale for diffusive motion in the absence of external driving ($\omega = 0$) for which $\tilde{D}_0 = 0.6$. The vertical gray bar indicates the transition from diffusive to directed transport. (b) The corresponding crossover length $\tilde{l}^* = \tilde{D}/|\tilde{V}|$ at which both time scales are equal, $\tilde{t}_v = \tilde{t}_d$, is plotted as a function of the frequency using the data from figs. 2(a), (c) for $m = 0$. (c) The time scales as a function of the transport length for parallel motion ($\tilde{A}_z = 0.5$ and $\tilde{A}_x = 0$) and for $\tilde{d} = 0.2$ with $\tilde{\omega} = 162$, $\tilde{V} = -0.81$, and $\tilde{D} = 1.78$. (d) The crossover length $\tilde{l}^* = \tilde{D}/|\tilde{V}|$ as a function of frequency for parallel motion using the data shown in figs. 4(a), (c) for $m = 0$.

fixed $\tilde{\chi} = 0.5$ and a distance $\tilde{d} = 0.2$. As opposed to perpendicular ratchet motion in fig. 2, we observe negative velocity for all values of m, *i.e.* we obtain particle transport to the left. For the interlocked case, $m = 1$, and the flat case, $m = 0$, the velocity decreases with increasing the frequency to a minimum, as shown in fig. 4(a), and simultaneously the diffusivity shown in fig. 4(c) exhibits a maximum. The overall diffusivity is enhanced compared to the equilibrium case $\tilde{\omega} = 0$ for which $\tilde{D} = 0.05$ for $m = 0$ and $\tilde{D} = 0.18$ for $m = -1$. In particular, the flat structure $m = 0$ leads to diffusivities $\tilde{D} > 1$ that are significantly larger than for free diffusion, which is obtained in the limit of large surface separations, in which case $\tilde{D} = 1$. Changing the surface structure to $m = -1$ (fig. 4(b), bottom) leads to suppressed transport with small negative velocities and a small diffusivity that only weakly depends on the frequency. We conclude that parallel motion of the oscillating surface can greatly enhance the diffusive transport of the nanoparticle while it leads to a negative average velocity, *i.e.*, directed transport to the left. This raises the question of what the dominating mode of transport for parallel motion is, a question we will address later on.

In fig. 5 we give a pictorial explanation for the difference between perpendicular and parallel oscillatory surface motion and the resulting flashing and pushing ratchet effects, respectively. Perpendicular ratchet motion, illustrated in fig. 5(a), causes an effect similar to what is known as the flashing ratchet effect [5, 27]. In contrast to previous theoretical models, here we consider a moving ratchet-shaped surface and two-dimensional particle motion instead of a ratchet potential in one dimension that is switched on and off. However, the mechanism of alternating particle localization and diffusion over a barrier is similar, including the necessary condition of a spatial symmetry breaking of the potential landscape. As seen in fig. 5(a), the perpendicular ratchet motion leads to particle transport to the right, which means that particles in step ii) diffuse from the minima over the steep flanks and are then in step iii) pushed down the shallow flanks to the right. Parallel ratchet motion, illustrated in fig. 5(b), causes a pushing ratchet effect. Due to spatial asymmetry, particles are in step i) predominantly pushed to the left by the steep flanks and in step ii) diffuse over the barrier of the shallow flanks to the next minimum on the left.

3.2 Diffusive vs. directed transport

In order to illustrate the difference between directed and diffusive transport, we plot in fig. 6(a) the characteristic time scale for directed motion, $\tilde{t}_v = \tilde{l}/|\tilde{V}|$, and for diffusive motion, $\tilde{t}_d = \tilde{l}^2/\tilde{D}$, as a function of the transport length $\tilde{l}$ using the maximal velocity $\tilde{V} = 0.18$ (at $\tilde{\omega} = 113$), obtained from fig. 2(a) for perpendicular surface motion and $m = 0$, where the diffusivity is $\tilde{D} = 0.7$. For short transport length less than about $\tilde{l} = 3.8$, diffusive transport, shown as a dashed line in fig. 6(a), is more effective, as indicated by a shorter characteristic time, compared to directed transport shown as a solid line. At a length $\tilde{l}^* = \tilde{D}/\tilde{V}$, indicated by a vertical gray bar in fig. 6(a), both times scales are equal, $\tilde{t}_v = \tilde{t}_d$. For a larger transport length directed motion leads to a smaller characteristic time compared to diffusive transport. For comparison, we also show the diffusive time in the absence of oscillatory surface motion, $\tilde{t}_0 = l^2/\tilde{D}_0$. In fig. 6(b), the crossover length $\tilde{l}^* = \tilde{D}/|\tilde{V}|$ is shown as a function of frequency $\tilde{\omega}$

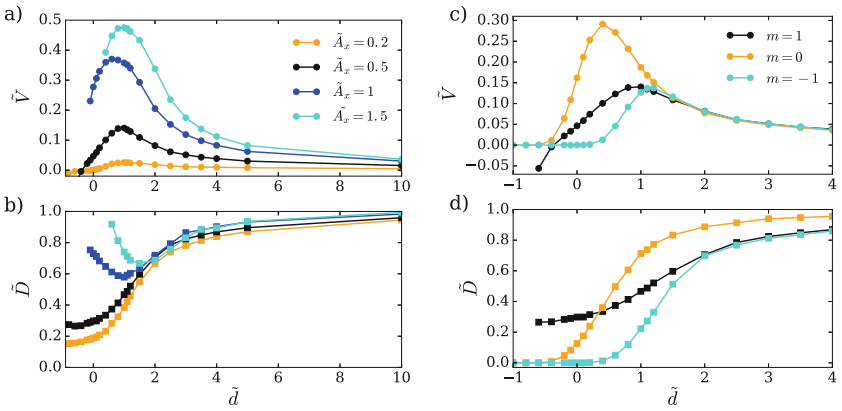

Fig. 7. A rigid particle under perpendicular ratchet motion with fixed frequency $\tilde{\omega} = 100$. For the interlocked case, $m = 1$, the (a) average velocity $\tilde{V}$ and the (b) diffusivity $\tilde{D}$ are plotted as a function of surface separation $\tilde{d}$ for a few different oscillation amplitudes $\tilde{A}_x$. The optimal distance for the enhanced transport of the particle to the right is about $\tilde{d} = 1$ at which $\tilde{V}$ exhibits a maximum. With increasing the amplitude $\tilde{A}_x$ the transport of the particle is more pronounced and the average velocity increases. For small amplitudes the diffusivity in (b) monotonically increases towards the free diffusion limit. Large amplitudes lead to a minimum in the diffusivity at distances $\tilde{d}$ that are slightly larger than the optimal distances in terms of particle velocity in (a). (c) For a fixed amplitude $\tilde{A}_x = 0.5$ the velocity is shown for different values of m and varying distance $\tilde{d}$. Maximal velocity and (d) diffusivity is observed for the flat case, $m = 0$ due less surface overlap.

for the same parameters used in fig. 6(a). We see that the crossover length exhibits a broad minimum at a frequency of about $\tilde{\omega} = 100$. For the case of parallel motion with $\tilde{A}_x = 0.5$ and $\tilde{A}_z = 0$, shown in figs. 6(c), (d), the transition from diffusive transport to the regime of directed transport occurs at a shorter time scale and at a smaller transport length $\tilde{l}^*$ compared to perpendicular motion. Note that we use different surface separations: $\tilde{d} = 1$ for perpendicular and $\tilde{d} = 0.2$ for parallel motion. The diagram in fig. 6(d) shows that the crossover length only weakly depends on the frequency of the parallel oscillating surface; only for large $\tilde{\omega} > 400$ the diffusive regime becomes dominant and $\tilde{l}^*$ increases.

3.3 Influence of particle size and surface structure

The investigation of the effect of different distances $\tilde{d}$ between the oscillating surface and the resting surface in our model presents a way to determine the influence of particle size on particle transport. In figs. 7(a), (b) we show results for the average particle velocity $\tilde{V}$ and diffusivity $\tilde{D}$, respectively, for the interlocked case, $m = 1$, fixed perpendicular frequency $\tilde{\omega} = 100$, and a few different values of the oscillation amplitude $\tilde{A}_x$. Small distances $\tilde{d} \leq 0$ lead to particle trapping due to confinement in the interlocked sawtooth surfaces characterized by small average velocities and small diffusivities. The optimal distance in terms of particle transport to the right is at about $\tilde{d} = 1$, which corresponds to twice the corrugation amplitude $\tilde{\chi} = 0.5$. This means that transport is most pronounced when the surfaces are close but not overlapping in order to prevent the particle from being trapped. For larger distances $\tilde{d} > 10$ the free diffusion limit is approached with vanishing average velocity and diffusivity $\tilde{D} = 1$, fig. 7(b). The overall average velocity in fig. 7(a) increases with increasing amplitude $\tilde{A}_x$. The diffusivity in fig. 7(b) monotonically increases with $\tilde{d}$ only for small amplitudes $\tilde{A}_x$. For $\tilde{A}_x \geq 1$ the diffusivity exhibits a minimum at about $\tilde{d} = \tilde{A}_x$. In figs. 7(c), (b) results are presented for a fixed amplitude $\tilde{A}_x = 0.5$ and different resting surface structures $m = 1, 0, -1$. The largest velocity and diffusivity is observed for the flat case. Only for small distances $\tilde{d} < 0.4$ the interlocked case ($m = 1$) yields a finite diffusivity of $\tilde{D} \approx 0.3$ whereas the other cases $m = 0, -1$ approach vanishing diffusivity when the surface distance decreases. Noticeably, negative velocities are observed for the interlocked case for very small $\tilde{d} \leq -0.4$ with strong surface overlap. This is an example of current reversal [25] induced by the variation of a system parameter that does not change the symmetry of the system.

The effect of different corrugation amplitudes $\tilde{\chi}$ of the sawtooth structure is illustrated in figs. 8(a), (b) showing the average velocity and diffusivity as a function of $\tilde{\chi}$ for different structure parameters $m = 1, 0$. The distance between the ratchet and resting surface is set to $\tilde{d} = 1$ and perpendicular motion is applied with fixed amplitude $\tilde{A}_x = 0.5$ and frequency $\tilde{\omega} = 100$. The average velocity in fig. 8(a) vanishes for low as well as for large values of $\tilde{\chi}$ with a maximum at $\tilde{\chi} = 0.4$ ($\tilde{\chi} = 0.5$) for $m = 1$ ($m = 0$). Note that our simulation results thus suggest an optimal nanoparticle transport into hair follicles for a corrugation amplitude of $\chi = 2\,\mu$m (for $L = 5\,\mu$m), which is larger than the typical cuticular hair thickness of about $0.6\,\mu$m [12] that can be estimated from the microscopic image in fig. 1(a). The diffusivity shown in fig. 8(b) monotonically decreases from the free diffusion value $\tilde{D} = 1$ for $\tilde{\chi} = 0$ to very small values for large $\tilde{\chi} = 0$, since the particle gets trapped between the surfaces.

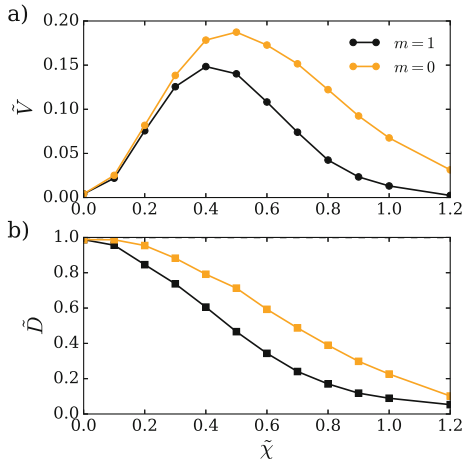

Fig. 8. A rigid particle subject to perpendicular ratchet motion with fixed $\tilde{d} = 1$, $\tilde{A}_x = 0.5$ and $\tilde{\omega} = 100$. (a) Average velocity and (b) diffusivity as a function of corrugation amplitude $\tilde{\chi}$ for the structure parameters $m = 1$ (black) and $m = 0$ (orange).

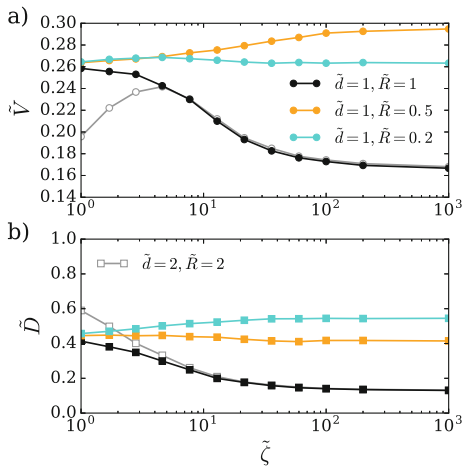

Fig. 9. An elastic nanoparticle is modeled via eq. (10) as a harmonic dumbbell of length $\tilde{R}$. Subject to perpendicular ratchet motion with fixed $\tilde{A}_x = 0.5$, $\tilde{\omega} = 100$, $\tilde{\chi} = 0.5$, $\tilde{d} = 1$, and $m = 0$, the (a) average velocity as a function of rigidity $\tilde{\zeta}$ monotonically decreases for a large particle with $\tilde{R} = 1$ (black) and increases for a slightly smaller particle radius $\tilde{R} = 0.5$ (orange). For very small $\tilde{R} = 0.2$ (cyan), the rigidity only weakly influences the particle velocity. For a larger distance $\tilde{d} = 2$ and radius $\tilde{R} = 2$ (gray open symbols) the velocity first increases with the rigidity to a maximum until it collapses with the black curve. (b) The diffusivity is larger for smaller particles. Whereas the largest particles exhibit a decreasing diffusivity with increasing the rigidity, small particles show increasing diffusivity when they become stiffer.

3.4 Influence of particle elasticity

In order to model an elastic nanoparticle we use a harmonic dumbbell with the potential energy eq. (10). The dumbbell length $\tilde{R}$ corresponds to the particle size and the rescaled spring constant $\tilde{\zeta} = \tilde{\zeta}R^2/\mathrm{kT}$ corresponds to the particle rigidity. In fig. 9 we present results for an elastic particle of different size $\tilde{R}$ subject to perpendicular ratchet motion with fixed amplitude $\tilde{A}_x = 0.5$ and frequency $\tilde{\omega} = 100$. The corrugation amplitude is $\tilde{\chi} = 0.5$ and the resting surface is flat, $m = 0$. For a small surface distance $\tilde{d} = 1$ and a comparable particle size $\tilde{R} = 1$ the average velocity, shown as black symbols in fig. 9(a), monotonically decreases with increasing the rigidity $\tilde{\zeta}$. Interestingly, the velocity for $\tilde{d} = 2$ and $\tilde{R} = 2$ (also giving rise to $\tilde{R}/\tilde{d} = 1$), shown as gray open symbols, first increases to a maximum around $\tilde{\zeta} = 5$ and for a larger rigidity collapses with the black line. In contrast, a slightly smaller particle with $\tilde{R} = 0.5$, shown for $\tilde{d} = 1$ as orange symbols in fig. 9, exhibits a larger average velocity when it becomes stiffer. The velocity of a very small particle with $\tilde{R} = 0.2$, cyan symbols in fig. 9, only weakly depends on the particle rigidity. The diffusivity, shown in fig. 9(b), for large particles decreases as a function of the rigidity and smaller particles display slightly increasing diffusivity when they become stiffer.

With respect to nanoparticle transport into hair follicles, the case of particles that are of the same size as the distance between hair and follicle surfaces is probably the most relevant. Hence, we conclude that in terms of directed transport and diffusion, flexible particles are expected to penetrate deeper into the hair follicle, an observation that is consistent with experiments comparing follicular penetration of rigid and flexible liposomes [28].

4 Summary and conclusion

In the present study, Brownian dynamics simulations are employed to obtain average velocities and diffusivities for the motion of a nanoparticle in a two-dimensional channel, where one of the two corrugated channel surfaces is oscillating. For simplicity, we only consider pure perpendicular motion and pure parallel motion of the oscillating surface, more realistic scenarios might involve a superposition of both modes of motion.

The perpendicular motion causes a flashing ratchet effect that rectifies the particle motion to the right, *i.e.* down the shallow flank of the oscillating surface. We determine the optimal driving frequency, the optimal particle size, and the optimal corrugation amplitude of the oscillating surface that yield the most efficient particle transport. In particular, particles exhibit maximal velocity when the surface separation roughly corresponds to the particle size and the corrugation amplitude corresponds to half the surface separation. The surface structure of the resting channel surface has a minor effect on the frequency dependence of the average velocity, but the diffusivity is much larger for the flat structure compared to corrugated surfaces because less confinement allows for more space for the particle to diffuse. Consequently, the optimal particle size is smaller for the flat resting surface structure.

Besides the directed transport mechanism, we also find enhanced diffusive motion induced by the perpendicular ratchet motion. We determine the crossover from the diffusive regime to the regime where directed transport dom-

inates. Since this crossover occurs for intermediate frequencies at a transport length of only $l^* \approx 5L$, where L is the periodicity of the oscillating surface, we conclude that for typical transport applications, *i.e.* $l \gg L$, the directed transport mechanism is more important than diffusion.

Parallel motion of the oscillating surface induces a distinct transport mechanism that we describe as pushing ratchet effect, which leads to directed particle motion to the left, *i.e.* in the opposite direction compared to perpendicular ratchet motion. This effect is most pronounced for the flat structure of the resting surface, leading to large negative velocities. In addition, we observe a significant enhancement of the diffusivities, which becomes even larger than for free diffusion. To what extent this diffusivity enhancement dominates compared to the directed transport depends on the total distance the particle has to move.

Elasticity of particles is included in the last part and we determine the transport properties for perpendicular ratchet motion. For a small channel surface separation and comparable particle size, we find that elastic particles exhibit larger velocities and diffusivities compared to rigid particles. This behavior changes when the particle size becomes smaller: small elastic particles show less efficient transport than small rigid particles. The non-monotonic behavior of the average velocity as a function of rigidity for large surface separation indicates a complex interplay between rigidity and other model parameters.

Financial support from the DFG Collaborative Research Center 1112 – "Nanocarriers: Architecture, Transport and Topical Application of Drugs for Therapeutic Use" is acknowledged.

References

1. A. Ajdari, J. Prost, C.r. Acad. Sci. Ser. II **315**, 1635 (1992).
2. R. Dean Astumian, Science **276**, 917 (1997).
3. Frank Jülicher, Armand Ajdari, Jacques Prost, Rev. Mod. Phys. **69**, 1269 (1997).
4. Andrea Parmeggiani, Frank Jülicher, Armand Ajdari, Jacques Prost, Phys. Rev. E **60**, 2127 (1999).
5. Peter Reimann, Phys. Rep. **361**, 57 (2002).
6. Michael Pycraft Hughes, J. Phys. D: Appl. Phys. **37**, 1275 (2004).
7. P. Hänggi, F. Marchesoni, F. Nori, Ann. Phys. **14**, 51 (2005).
8. Peter Hänggi, Fabio Marchesoni, Rev. Mod. Phys. **81**, 387 (2009).
9. I.M. Kulić, R. Thaokar, H. Schiessel, Europhys. Lett. **72**, 527 (2005).
10. I.M. Kulic, P.C. Nelson, EPL **81**, 18001 (2008).
11. Kazuo Kitamura, Makio Tokunaga, Atsuko Hikikoshi Iwane, Toshio Yanagida, Nature **397**, 129 (1999).
12. J. Lademann, F. Knorr, H. Richter, S. Jung, M.C. Meinke, E. Rühl, U. Alexiev, M. Calderon, A. Patzelt, J. Innov. Opt. Health Sci. **08**, 1530004 (2015).
13. B. Nordén, Y. Zolotaryuk, P.L. Christiansen, A.V. Zolotaryuk, Phys. Rev. E **65**, 011110 (2001).
14. L. Mahadevan, S. Daniel, M.K. Chaudhury, Proc. Natl. Acad. Sci. **101**, 23 (2004).
15. I.M. Kulic, M. Mani, H. Mohrbach, R. Thaokar, L. Mahadevan, Proc. R. Soc. B: Biol. Sci. **276**, 2243 (2009).
16. C.J. Olson Reichhardt, C. Reichhardt, *Ratchet effects in active matter systems*, arXiv:1604.01072 [cond-mat.soft].
17. T.-Q. Truong, N.-T. Nguyen, *Simulation and optimization of tesla valves*, in *Technical Proceedings of the 2003 Nanotechnology Conference and Trade Show*, Vol. **1** (2003) p. 178.
18. Tarl W. Prow, Jeffrey E. Grice, Lynlee L. Lin, Rokhaya Faye, Margaret Butler, Wolfgang Becker, Elisabeth M.T. Wurm, Corinne Yoong, Thomas A. Robertson, H. Peter Soyer, Michael S. Roberts, Adv. Drug Deliv. Rev. **63**, 470 (2011).
19. Lukas Bogunovic, Ralf Eichhorn, Jan Regtmeier, Dario Anselmetti, Peter Reimann, Soft Matter **8**, 3900 (2012).
20. J. Lademann, H. Richter, M.C. Meinke, B. Lange-Asschenfeldt, C. Antoniou, W.C. Mak, R. Renneberg, W. Sterry, A. Patzelt, Skin Pharmacol. Physiol. **26**, 227 (2013).
21. Juergen Lademann, Heike Richter, Alexa Teichmann, Nina Otberg, Ulrike Blume-Peytavi, Javiana Luengo, Barbara Weiss, Ulrich F. Schaefer, Claus-Michael Lehr, Roger Wepf, Wolfram Sterry, Eur. J. Pharm. Biopharm. **66**, 159 (2007).
22. Juergen Lademann, Alexa Patzelt, Heike Richter, Christina Antoniou, Wolfram Sterry, Fanny Knorr, J. Biomed. Opt. **14**, 021014 (2009).
23. Leszek J. Wolfram, J. Am. Acad. Dermatol. **48**, S106 (2003).
24. M. Ossadnik, H. Richter, A. Teichmann, S. Koch, U. Schäfer, R. Wepf, W. Sterry, J. Lademann, Laser Phys. **16**, 747 (2006).
25. Roland Bartussek, Peter Hänggi, Jürgen G. Kissner, Europhys. Lett. **28**, 459 (1994).
26. M. Ito, Arch. Dermatol. Res. **279**, 112 (1986).
27. A.L.R. Bug, B.J. Berne, Phys. Rev. Lett. **59**, 948 (1987).
28. Sindy Trauer, Heike Richter, Judith Kuntsche, Rolf Büttemeyer, Manfred Liebsch, Michael Linscheid, Alfred Fahr, Monika Schäfer-Korting, Jürgen Lademann, Alexa Patzelt, Eur. J. Pharm. Biopharm. **86**, 301 (2014).